Supporting Information

Woolley et al. 10.1073/pnas.1217832110

SI Methods

Mouse Experiment. ***Subjects.*** Eight-week-old female C57BL/6J mice (Centre D'Elevage Janvier) were group housed (five to seven mice per cage) in standard cages with wood-shaving bedding. Food and water were available ad libitum, and mice were handled for 1 wk (tail coloring) before the start of behavioral testing. The housing environment was temperature and humidity controlled with a 12-h light–dark cycle (lights on at 8:00 AM). Behavioral testing was performed during the light phase. All procedures were approved by the ethical research committee of KU Leuven in accordance with the Declaration of Helsinki.

Behavioral procedures. Mice were trained on the hidden platform version of the Morris water maze. The test apparatus consisted of a large circular pool (diameter 150 cm, height 33 cm) filled with water (25–26 °C) to a depth of 16 cm. Water was made opaque with nontoxic white paint to prevent animals from seeing a transparent circular platform (diameter 15 cm, height 15 cm) submerged 1 cm beneath the surface. The platform was located at a fixed position 25 cm from the nearest pool wall. The pool was located in an elevated position in the center of a well-lit room with various distinct visual cues. Each trial began at one of four starting locations by placing the mouse at the edge of the pool facing toward the center. During trials the experimenter remained seated at a fixed location. When a trial was not completed in 2 min the mouse was guided to the platform and remained there for 15 s.

All mice arrived in the laboratory at the same time and were handled daily. From the start of the experiment all cages were transferred to the training room each day. Experimental mice were trained to find the hidden platform for 3 d (one session of four trials per day) and 30 d (two sessions of four trials per day for the first 25 d of training, then one session of four trials per day for the remaining 5 d; 5 consecutive training days were followed by 2 rest days). Trials in each session were separated by a 15-min break, and when two sessions were performed on a single day they were separated by 2 h. Free-swimming control mice (3 d and 30 d) explored the same environment except that the hidden platform and distal cues were removed. With distal cues present in the free-swimming condition goal-directed navigation and learning remains possible (albeit not learning of an escape platform location). Therefore, the likelihood of achieving true free-swimming performance (i.e., not goal-directed) was optimized by the removal of distal cues. Nonswimming caged control mice did not receive any water maze training but were always transferred between housing and training rooms together with the other 4 groups during the 30 d testing period. All mice were 15 wk old on the final day of training.

Behavior was recorded using Ethovision video tracking equipment and software (Noldus). Overall task performance was evaluated by calculating the time taken to find the hidden platform (latency). Spatial performance was evaluated by calculating the average distance between the mouse and the hidden platform (search proximity). A repeated measures one-way ANOVA was used to test for learning-related changes in the experimental groups. The α-level was set to 0.05.

Quantitative in situ hybridization to determine **zif268** ***expression.*** *zif268* in situ hybridization was performed using previously established methods in our laboratory (1). Briefly, animals where killed at the age of 15 wk by cervical dislocation 45 min after the final training trial, and brains were immediately frozen in 2-methylbutane (Merck) at a temperature of −40 °C. Coronal sections (25 μm) were cut on a cryostat (Microm HM 500 OM) and mounted onto 0.1% poly-L-lysine coated slides (Sigma-Aldrich). A series of brain sections covering the entire rostrocaudal extent of the striatum/anterior cingulate (medial prefrontal cortex) and hippocampus were collected (2) and kept at −30 °C. Tissue was postfixed in 4% (vol/vol) paraformaldehyde in 0.12 M phosphoric acid in PBS (0.1 M, pH 7.4, 30 min, 4 °C; 0.9% NaCl), dehydrated [50% (vol/vol), 70% (vol/vol), 98% (vol/vol), 100% (vol/vol), 5 min], and delipidated [100% (vol/vol) chloroform, 10 min]. The mouse-specific synthetic *zif268* probe (NM_007913.5, sequence: 5′ccgttgctcagcatcatctcctccagyttrgggtagttgtcc3′) was end-labeled with 33P-dATP (New England Nuclear) using terminal deoxynucleotidyl transferase (Invitrogen). Unincorporated nucleotides were removed using mini Quick Spin columns (Roche Diagnostics). The radioactive labeled probe was mixed with a hybridization mixture [50% (vol/vol) formamide, 4× standard saline citrate, 1× Denhardt's solution, 10% (wt/vol) dextran sulfate, 100 μg/mL Herring sperm DNA, 250 μg/mL tRNA, 60 mM DTT, 1% (wt/vol) *N*-lauryl-sarcosine, and 26 mM NaHPO4 (pH 7.4)] and applied to a series of dehydrated sections with overnight incubation at a temperature of 37 °C. The next day, the sections were rinsed in 1× standard saline citrate buffer at 42 °C, air-dried, and apposed to an autoradiographic film (Kodak) together with a [14C] microscale (GE Healthcare). Films were developed 3 wk later in Kodak D19 developing solution and fixed in Rapid fixer (Ilford Hypam).

Autoradiographic images were scanned (CanoScan LiDE 600F; Canon), and optical densities (mean gray value per pixel) were quantified with ImageJ (image processing and analysis in Java; National Institutes of Health). Optical density was measured in three brain sections per mouse along the rostrocaudal axis for each target region. Striatum and medial prefrontal cortex slices were taken from +1.10 mm to +0.38 mm relative to bregma (Fig. S4*A*) and CA1 slices from −1.58 mm to −2.54 mm relative to bregma (2). Within striatum we targeted dorsolateral and superior dorsomedial subdivisions (Fig. S4*B*). The template of the striatal and medial prefrontal cortex compartments was drawn bilaterally over brain sections. Mean gray values were averaged across hemispheres and brain slices, resulting in a single data point for each region per animal. A one-way between-groups ANOVA was use to test differences in immediate early gene (IEG) expression between the caged control group and all experimental and control groups. To test for learning-related changes in IEG expression mean gray values were entered into an ANOVA (2 conditions × 2 learning phases). For all analyses the α-level was set to 0.05 and Bonferroni correction applied to post hoc tests. Statistical analyses were performed in Statistica 9 (StatSoft).

Corticosterone levels. Comparison of corticosterone levels ensured that between-group differences in IEG expression were not confounded by stress. After decapitation, blood (0.3–0.5 mL) was collected in heparin-coated Eppendorf tubes (heparin lithium salt from porcine intestinal mucosa, Sigma-Aldrich; concentration coating: ~22 U per tube) and centrifuged (845 × *g*, 3 °C, 15 min). Plasma was transferred to new tubes and stored at −20 °C. Plasma corticosterone levels were measured using a commercially available double antibody RIA (IDS Ltd.). The intraassay coefficient for corticosterone was 3.9%. A one-way between-groups ANOVA revealed that corticosterone levels did not differ significantly between groups ($F_{4,26} = 1.462$, $P = 0.24$; Fig. S5).

Human Experiment. ***Subjects.*** Eighteen female subjects (aged 20–28 y, mean age 23.1 y) participated in the fMRI study. All were right-handed with no history of neurological disease. Before testing, subjects were required to provide written informed consent to the procedures, which were approved by the Ethics

Committee of KU Leuven in accordance with the Declaration of Helsinki.

Task. A custom virtual environment analogous to the Morris water maze was constructed in Blender (www.blender.org) and rendered in MATLAB (2007b; The Mathworks). The environment consisted of a circular pool [diameter = 16 virtual reality units (vru), height = 0.5 vru] situated 0.5 vru above ground level in the center of a square room (length = 20 vru, height = 8 vru). Within the pool was a hidden platform 1.6 vru in diameter. There was only one distinguishing feature in the environment: a black cross located on a wall approximately half way between the floor and the ceiling in the opposite corner of the room to the quadrant in which the hidden platform was located. Subjects viewed the room from a first-person perspective and moved around by pressing buttons on an MRI-compatible button box (Current Designs Inc.). Movement was restricted to either forward displacement or orienting (i.e., rotating left and right in the same position). A single button press resulted in a forward movement of 0.1 vru or rotation of 1.5°. Data were recorded at 25 Hz (Fig. S6*A*).

Trial procedures. Over the course of the experiment subjects performed "search" and "control" trials, which were designed to be compatible with our mouse water maze experiment. All trials began from one of four starting zones (separated by 90°) located at the perimeter of the pool, with the exact position within a given starting zone varying by ±10° from trial to trial. Subjects always faced the center of the pool at the beginning of the trial.

The goal of search trials was to navigate to the hidden platform as quickly and directly as possible. When the goal location was successfully intercepted the walls of the room turned green for 1 s, after which the subject remained at the same location for a further 3 s. During this 4-s period forward movement and orienting were not possible. The maximum time limit for search trials was 45 s. If a trial reached the maximum time limit the walls of the room turned red for 1 s, after which the subject remained in their final unsuccessful location for a further 3 s (forward movement and orienting were again not possible during this 4-s period).

During control trials subjects moved freely within the pool. No distinguishing features were present on the walls, preventing any goal-directed navigation. Control trials were matched to the average duration of search trials (between 10 and 20 s) and finished in a similar manner, with the only difference being that the color of the walls always turned blue (which did not relate to feedback provided during other trials). Fig. S6*B* shows screenshots.

A third trial type, "prediction" trials, required the subject to explicitly indicate where they thought the hidden platform was located via a button press. Analysis of prediction trials is not presented here because we focused on the conditions closest to the mouse experiment.

Experimental protocol. Four testing sessions were completed, each on a separate day. The first session familiarized subjects with the experimental procedures and trial order before scanning. During this session a limited number of trials were performed in a different environment from that used in the main experiment.

One or two days later subjects returned for the first scan session. From this session onward the environment and the location of the hidden platform was unchanged. Subjects performed 6 runs of trials, with each run lasting at least 8 min. The order of presentation of search, prediction, and control trials was determined as follows: each sequence always started with a search trial. An unsuccessful search trial was repeated until the hidden target zone was successfully intercepted. Once a successful search trial was completed, a prediction and control trial were presented next. The order in which the prediction and control trials were presented was randomized. The sequence was then repeated. The current trial type was always displayed in small text at the top of the screen. Subjects rested for 5–10 s between trials and were required to fixate on a white cross in the center of a black screen.

A second identical scan session was performed 6–8 d after the first. Between scan sessions subjects performed a training session during which only behavioral data were acquired. The behavioral training session also consisted of six runs of trials each lasting 8 min.

Resting-state protocol. In addition to acquiring task-related fMRI data, subjects were also scanned for 7 min in a resting state before the onset of task performance. Subjects were required to fixate on a white cross in the center of a black screen and were instructed to relax and think of nothing in particular.

Behavioral analysis. The same behavioral measures as those previously described in mouse (i.e., latency and search proximity) were also used to quantify performance on the virtual water maze. To test for learning within each session we conducted a one-way repeated-measures ANOVA (runs 1–6). Statistical analyses were performed in Statistica 9. The α-level was set to 0.05.

Image acquisition. A Siemens 3 T Magnetom Trio MRI scanner with 12-channel head coil was used for image acquisition. For all subjects, a high resolution T1-weighted structural image was acquired using a magnetization prepared rapid gradient echo sequence [repetition time (TR) 2,300 ms, echo time (TE) 2.98 ms, 1 × 1 × 1.1-mm voxels, field of view (FOV) 240 × 256, 160 sagittal slices]. Functional data (fMRI) were acquired with a descending gradient echo planar imaging (EPI) pulse sequence for T2*-weighted images (TR 3,000 ms, TE 30 ms, flip angle 90°, 50 oblique axial slices each 2.8 mm thick, interslice gap 0.028 mm, in-plane resolution 2.5 × 2.5 mm, 80 × 80 matrix).

Image preprocessing. Image preprocessing was conducted using SPM8 (Wellcome Department of Imaging Neuroscience, University College London). Functional images were spatially realigned and unwarped, slice time corrected to the middle slice (reference slice = 25), normalized to the standard EPI template of the Montreal Neurological Institute, resampled into 2-mm isotropic voxels, and spatially smoothed with an isotropic 8-mm full-width-at-half-maximum Gaussian kernel. Resting-state data were preprocessed in a similar manner, except functional images were not unwarped, resampled into 3-mm isotropic voxels, and spatially smoothed with an isotropic 5-mm full-width-at-half-maximum Gaussian kernel.

Statistical analysis of FMRI data. Search trials, control trials, and rest after control trials were modeled for each subject as boxcar functions convolved with the canonical hemodynamic response function within a first-level general linear model. The time series in each voxel was high-pass filtered at 1/160 Hz to remove low-frequency drifts. The contrasts search > rest and control > rest were specified separately for each run.

Contrasts were entered into a second-level random-effects ANOVA model with the factors trial type (search > rest and control > rest) and run (runs 1–6 and 13–18). The model was estimated under the assumption of dependent measurements and unequal variances. The *t*-contrast identifying areas responding more strongly to search than control trials was thresholded at $P < 0.05$, family-wise error (FWE) corrected for multiple comparisons within the whole brain, and only included clusters above 30 voxels.

Further analyses focused on the striatum, prefrontal cortex and hippocampus. Regions of interest (ROIs) were defined on the basis of a priori anatomical and functional criteria (see next section). For each of the ROIs created in striatum, medial prefrontal cortex, and hippocampus, the marsbar toolbox (3) was used to extract the mean contrast value of all voxels [i.e., an estimate of the hemodynamic response to either search or control trials (compared with rest) in the area of interest]. Unsmoothed images were used to avoid including signal from neighboring regions. To test for changes in activation over the course of learning, contrast values were entered into an ANOVA (2 trial types × 2 learning phases). Statistical analyses were performed in Statistica 9. The α-level was set to 0.05. Post hoc tests were Bonferroni corrected.

ROI definition. Caudate and putamen [defined by the Harvard-Oxford subcortical atlas (4)] activations were divided into dorsal/ventral and anterior/posterior subregions (Fig. S4*C*). Boarders were defined on the basis of prior knowledge regarding functional differences between subregions within the striatum (5). The dorsal/ventral division was defined as $z \geq 9$ (dorsal) and $z \leq 5$ (ventral) for the caudate and $z \geq 4$ (dorsal) and $z \leq 0$ (ventral) for the putamen. The anterior/posterior division was defined as $y \geq 2$ (anterior) and $y \leq -2$ (posterior) for both caudate and putamen. The gap between masks ensured that the signal from each voxel would only be included in one subdivision. According to these anatomical and functional criteria, the following bilateral striatal ROIs were created: dorsal posterior caudate, dorsal anterior caudate, ventral anterior caudate, dorsal posterior putamen, dorsal anterior putamen, and ventral anterior putamen (Fig. S4*D*).

The medial prefrontal cortex ROI in mouse was selected on the basis of its connectivity to dorsomedial striatum. For the human data analysis we used resting-state fMRI to identify voxels in prefrontal cortex functionally connected to dorsomedial striatum while at rest. Processing steps necessary to optimally prepare the data for functional connectivity analysis included band-pass filtering between 0.009 and 0.08 Hz, regression of global white matter and ventricle signals and their first derivatives, and regression of 3D motion parameters and their first derivatives (6). Whole-brain connectivity maps were created for all individual participants by calculating correlations between the average time course of voxels in dorsomedial striatum and all of the time courses of the brain voxels (6). After applying Fisher's *r*-to-*z* transformation to each correlation map, a random effects analysis was performed to reveal a pattern of functional connectivity that was consistent across subjects (7). Statistical significance was assessed at the voxel level by means of one-sample *t* tests, with a statistical threshold of $P < 0.05$ corrected for multiple comparisons by false discovery rate (FDR) (8). An ROI was then created for those voxels in the prefrontal cortex with (*i*) significant functional connectivity with dorsal posterior caudate at rest and (*ii*) a significantly higher response during search trials compared with control trials.

Although we did not find any voxels in hippocampus that responded more strongly to search trials than control trials in our whole-brain analysis, we further tested for differences between trial types in this region using a more sensitive approach. We performed a hierarchical cluster analysis with temporal correlation as a similarity metric and the average linkage function to compartmentalize hippocampus into functional subdivisions characterized by distinct resting-state activity (9, 10). This analysis revealed clusters in bilateral anterior, mid, and posterior hippocampus (Fig. S7). Subsequent analysis was only performed on the bilateral posterior hippocampus cluster, because this region is most likely to be engaged in spatial learning in human (11, 12).

SI Discussion

In dorsolateral striatum we found increased activity in both species during early and late phases of place learning, suggesting a contribution to task performance that was not learning phase specific. The dorsolateral striatum is typically associated with habitual or automatized behavior (13–16). Yin et al. (17) recently demonstrated with in vivo recordings that the dorsomedial and dorsolateral striatum were preferentially engaged during early and late learning phases of motor skill acquisition, respectively. On the basis of this evidence one would expect an increase in dorsolateral striatum activity specific to the late phase of water maze learning. However, they also found that lesions in dorsolateral striatum impaired both early and late phases of motor learning (17). Although the use of a motor task might have increased dependence on the dorsolateral striatum, simultaneous activity in dorsomedial and dorsolateral striatum was also recently observed during the early phase of a spatial learning task (18). Thus, our pattern of increased activation in both dorsomedial and dorsolateral striatum during early learning, followed by a decrease in dorsomedial striatum and no change in dorsolateral striatum in late learning, is consistent with the interpretation that functionally distinct processes in these striatal subdivisions develop in parallel, and not serially (17).

1. Van Brussel L, Gerits A, Arckens L (2011) Evidence for cross-modal plasticity in adult mouse visual cortex following monocular enucleation. *Cereb Cortex* 21(9):2133–2146.
2. Franklin KBJ, Paxinos G (2008) *The Mouse Brain in Stereotaxic Coordinates* (Elsevier Academic, San Diego, CA), 3rd Ed.
3. Brett M, Anton JL, Valabregue R, Poline JB (2002) Region of interest analysis using an SPM toolbox. *8th International Conference on Functional Mapping of the Human Brain, June 2–6, Sendai, Japan. NeuroImage* 16:497.
4. Makris N, et al. (1999) MRI-Based topographic parcellation of human cerebral white matter and nuclei II. Rationale and applications with systematics of cerebral connectivity. *Neuroimage* 9(1):18–45.
5. Postuma RB, Dagher A (2006) Basal ganglia functional connectivity based on a meta-analysis of 126 positron emission tomography and functional magnetic resonance imaging publications. *Cereb Cortex* 16(10):1508–1521.
6. Fox MD, et al. (2005) The human brain is intrinsically organized into dynamic, anticorrelated functional networks. *Proc Natl Acad Sci USA* 102(27):9673–9678.
7. Fox MD, Corbetta M, Snyder AZ, Vincent JL, Raichle ME (2006) Spontaneous neuronal activity distinguishes human dorsal and ventral attention systems. *Proc Natl Acad Sci USA* 103(26):10046–10051.
8. Genovese CR, Lazar NA, Nichols TE (2002) Thresholding of statistical maps in functional neuroimaging using the false discovery rate. *Neuroimage* 15(4):870–878.
9. Everitt BS, Landau S, Leese M (2001) *Cluster Analysis* (Arnold, London), 4th Ed.
10. Mantini D, et al. (2011) Default mode of brain function in monkeys. *J Neurosci* 31(36): 12954–12962.
11. Doeller CF, King JA, Burgess N (2008) Parallel striatal and hippocampal systems for landmarks and boundaries in spatial memory. *Proc Natl Acad Sci USA* 105(15): 5915–5920.
12. Burgess N, Maguire EA, O'Keefe J (2002) The human hippocampus and spatial and episodic memory. *Neuron* 35(4):625–641.
13. Balleine BW, O'Doherty JP (2010) Human and rodent homologies in action control: corticostriatal determinants of goal-directed and habitual action. *Neuropsychopharmacology* 35(1):48–69.
14. Tricomi E, Balleine BW, O'Doherty JP (2009) A specific role for posterior dorsolateral striatum in human habit learning. *Eur J Neurosci* 29(11):2225–2232.
15. Yin HH, Knowlton BJ (2006) The role of the basal ganglia in habit formation. *Nat Rev Neurosci* 7(6):464–476.
16. Yin HH, Knowlton BJ (2004) Contributions of striatal subregions to place and response learning. *Learn Mem* 11(4):459–463.
17. Yin HH, et al. (2009) Dynamic reorganization of striatal circuits during the acquisition and consolidation of a skill. *Nat Neurosci* 12(3):333–341.
18. Thorn CA, Atallah H, Howe M, Graybiel AM (2010) Differential dynamics of activity changes in dorsolateral and dorsomedial striatal loops during learning. *Neuron* 66(5): 781–795.

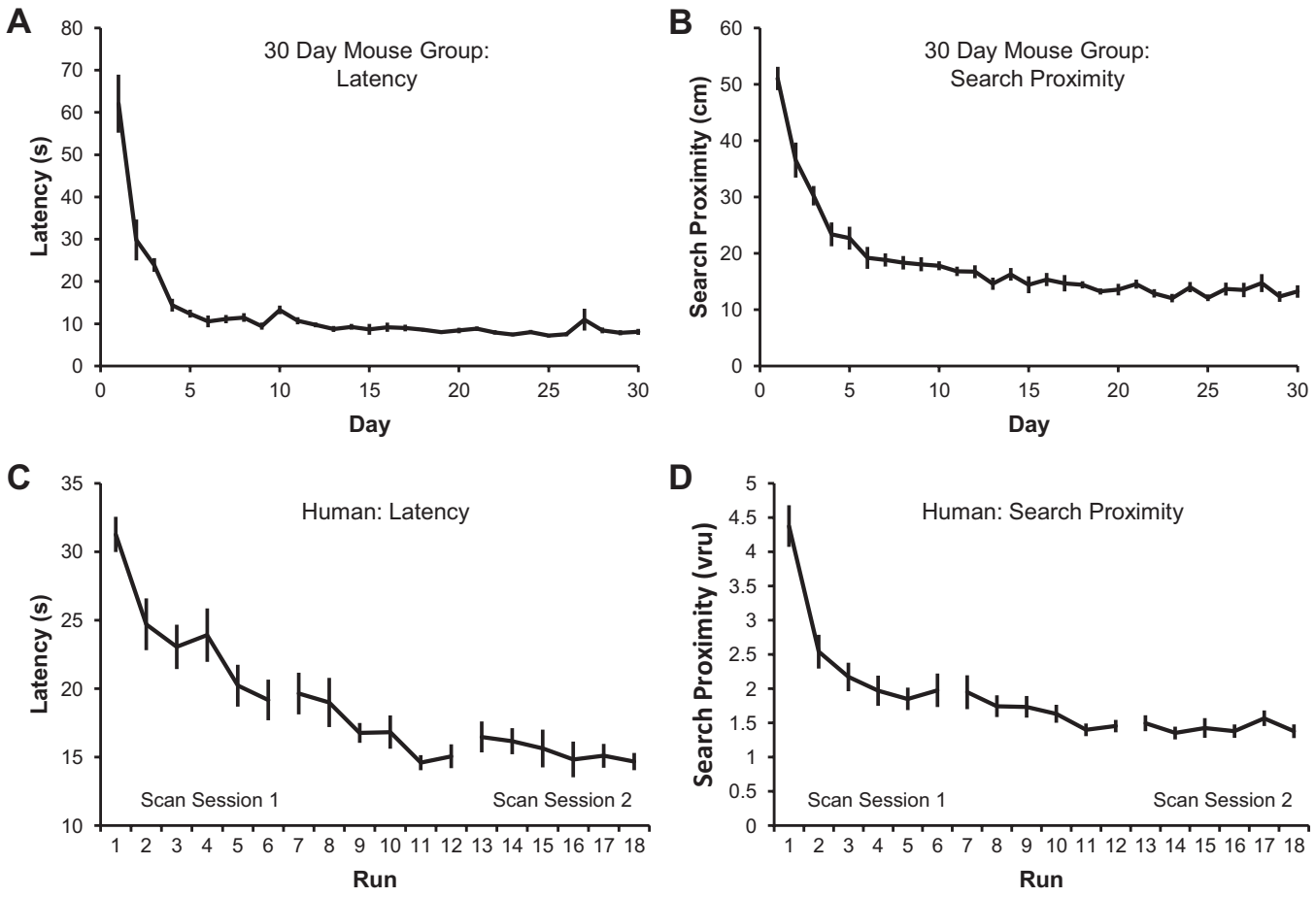

Fig. S1. Complete learning curves showing average performance across days for the 30-d group in mouse and runs for humans. Latency (*A*) and search proximity (*B*) are stable toward the end of training in the 30-d group. In human, latency (*C*) and search proximity (*D*) improve rapidly in scan session 1 (runs 1–6), show a small further improvement during overtraining outside the scanner (runs 7–12), and are stable in scan session 2 (runs 13–18). Error bars represent SEM.

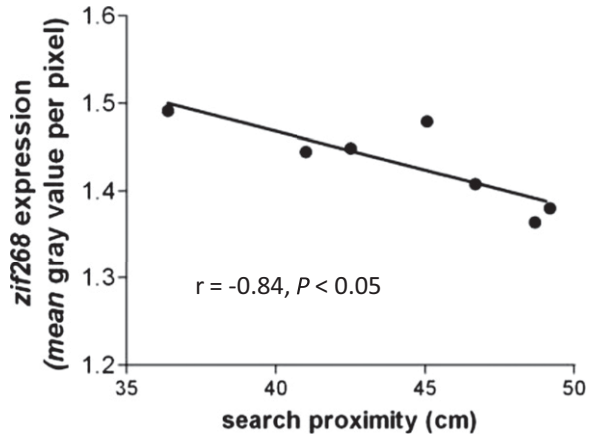

Fig. S2. *zif268* expression in medial prefrontal cortex during early learning was positively correlated with search proximity.

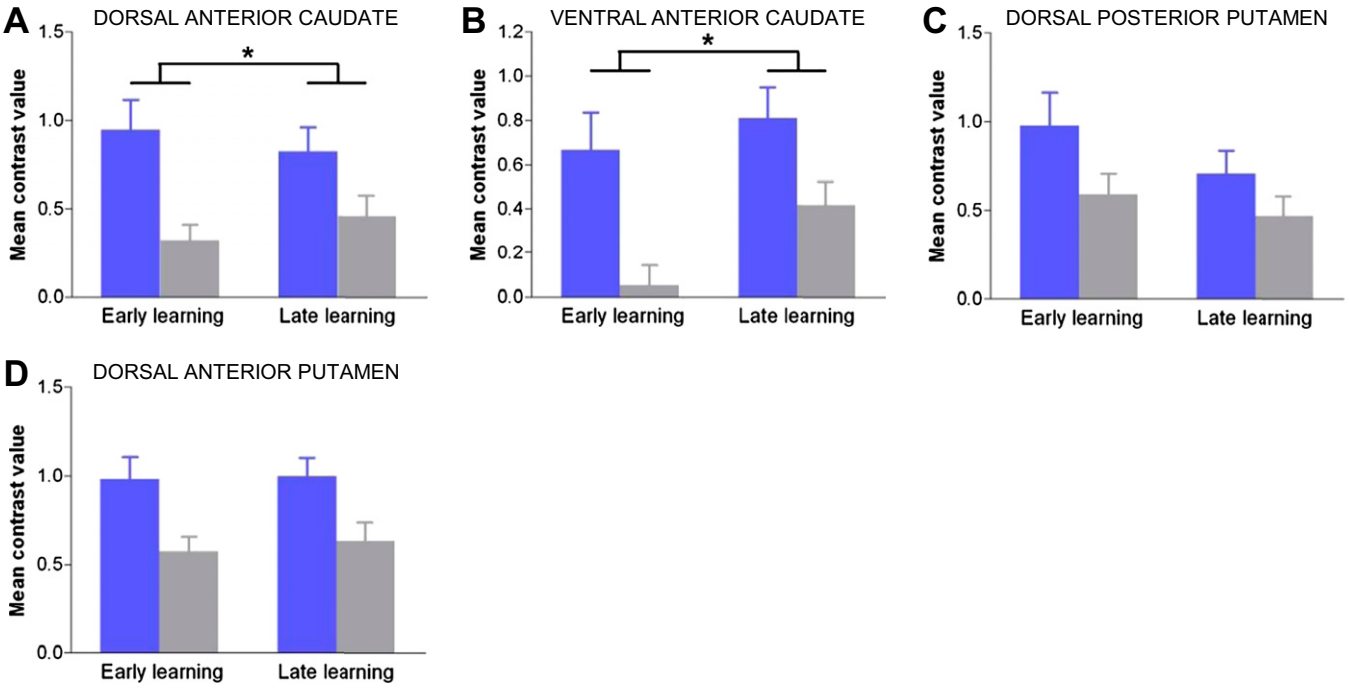

Fig. S3. Subdivisions in human striatum that did not show learning related changes in activity. Significant interactions were observed in dorsal anterior caudate ($F_{1,17} = 7.52$, $P < 0.05$) (*A*) and ventral anterior caudate ($F_{1,17} = 4.91$, $P < 0.05$) (*B*); however, these resulted from changes in activation on control trials and not search trials. Significant interactions were not observed in any of the dorsolateral subdivisions (*C* and *D*). There was a significant main effect of trial type in all striatal subdivisions, which was expected because these ROIs were initially selected based on this contrast. *$P < 0.01$.

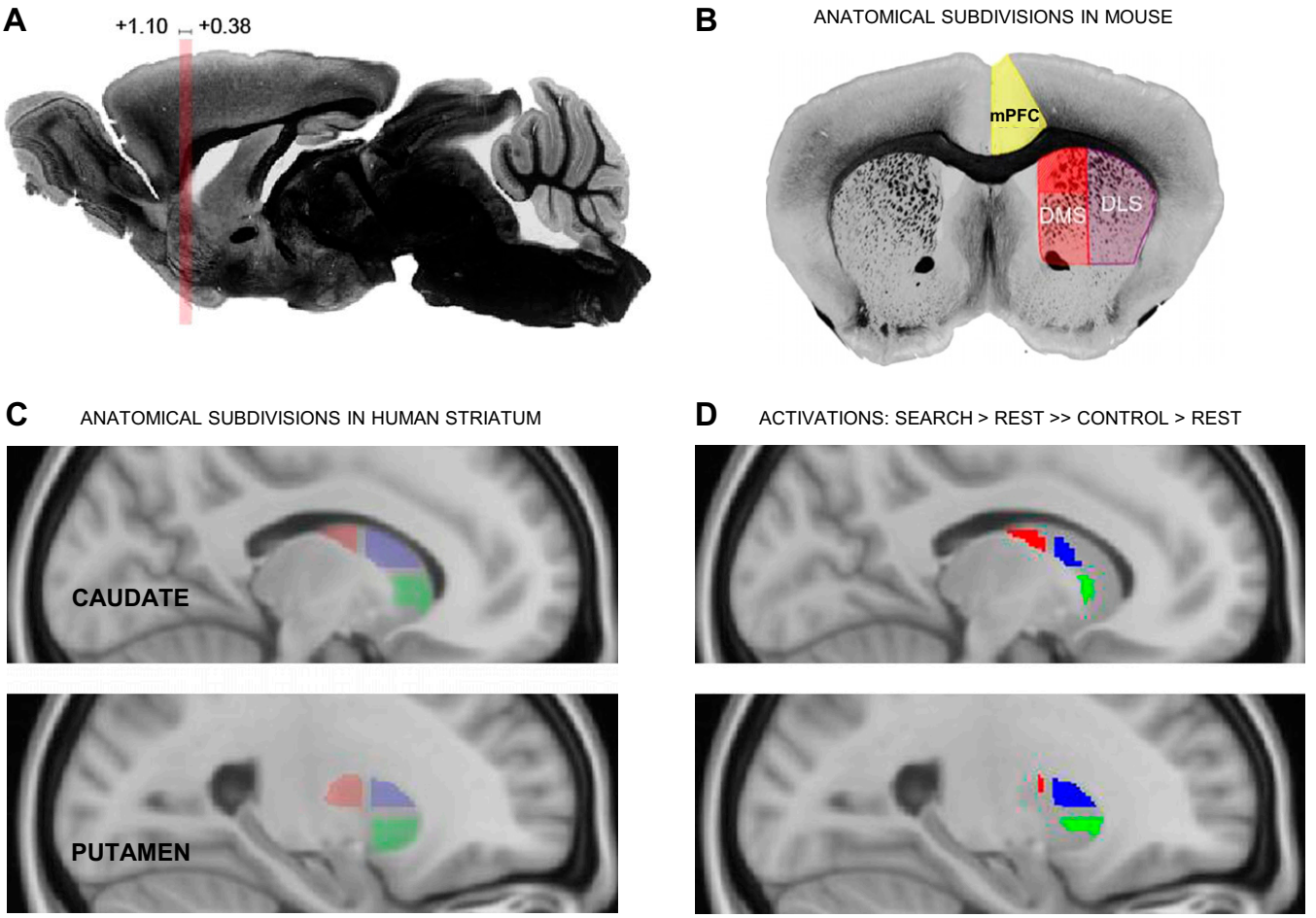

Fig. S4. Regions of interest. (*A*) *zif268* expression in the striatum and medial prefrontal cortex of mouse was measured in three brain sections along the rostrocaudal axis from +1.10 mm to +0.38 mm relative to bregma. (*B*) Dorsomedial striatum is shaded in red, with diagonal red lines indicating the superior subdivision reported in the present study. Dorsolateral striatum is shaded in purple and the medial prefrontal cortex in yellow. (*C*) Caudate ($x = 13$; also referred to as dorsomedial striatum) and putamen ($x = 24$; also referred to as dorsolateral striatum) in human were each subdivided into three regions. The dorsal posterior region is shaded in red, the dorsal anterior region in blue, and the ventral anterior region in green. (*D*) Clusters of voxels in each anatomical subdivision that responded more strongly in search trials than control trials compared with rest (FWE corrected, $P < 0.05$).

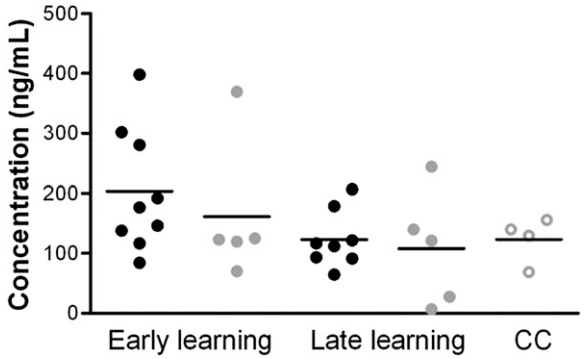

Fig. S5. Mouse corticosterone levels across all experimental and control groups were not significantly different. Solid black dots represent experimental animals (black dots), solid gray dots represent free-swimming controls, and open gray dots represent caged controls (CC).

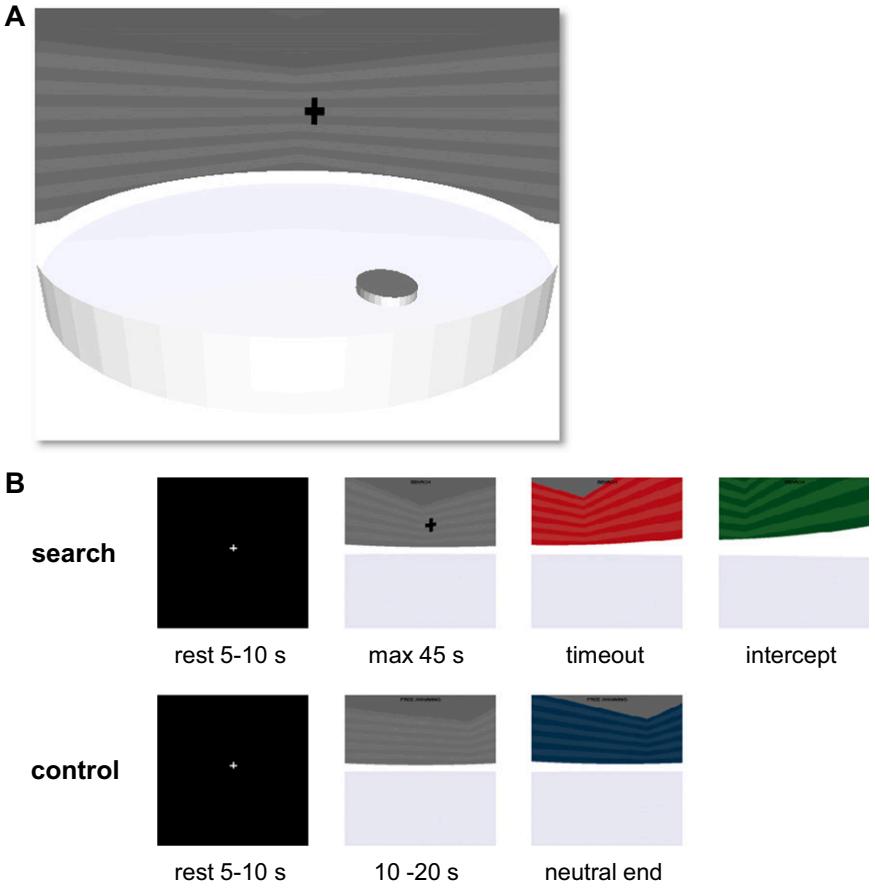

Fig. S6. Virtual water maze environment. (*A*) The virtual water maze viewed from an elevated position within the room showing the position of the hidden platform. Note that the platform was not visible at anytime during testing. (*B*) Order of events in search and control trials. Screenshots display a first-person view of the environment seen by the subject during testing. Feedback during trials was provided by the walls of the room changing color.

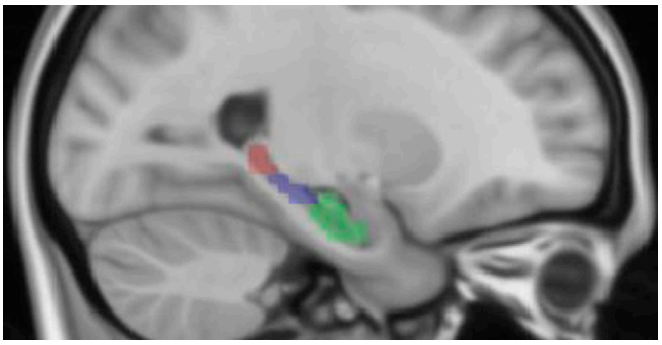

Fig. S7. Three anatomical subdivisions were defined in hippocampus ($x = -24$) on the basis of a hierarchical cluster analysis. The posterior region of hippocampus is shaded in red, the mid region in blue, and the anterior region in green. Only the (bilateral) posterior subdivision was used for further analysis.